Video Article

Quantitative Visualization of Leukocyte Infiltrate in a Murine Model of Fulminant Myocarditis by Light Sheet Microscopy

Linda Männ[1], Anika Klingberg[2], Matthias Gunzer[2], Mike Hasenberg[3]

[1]Department of Translational Skin Cancer Research, University of Duisburg/Essen

[2]Institute for Experimental Immunology and Imaging, University of Duisburg/Essen

[3]Imaging Center Essen, Electron Microscopy Unit, University Hospital of Essen

Correspondence to: Mike Hasenberg at mike.hasenberg@uni-due.de

URL: https://www.jove.com/video/55450
DOI: doi:10.3791/55450

Keywords: Medicine, Issue 123, light-sheet microscopy, myocarditis, whole-organ microscopy, chemical clearing, *in situ* antibody staining, CD11c.DTR, sterile inflammation

Date Published: 5/31/2017

Citation: Männ, L., Klingberg, A., Gunzer, M., Hasenberg, M. Quantitative Visualization of Leukocyte Infiltrate in a Murine Model of Fulminant Myocarditis by Light Sheet Microscopy. *J. Vis. Exp.* (123), e55450, doi:10.3791/55450 (2017).

Abstract

Light-sheet fluorescence microscopy (LSFM), in combination with chemical clearing protocols, has become the gold standard for analyzing fluorescently labelled structures in large biological specimens, and is down to cellular resolution. Meanwhile, the constant refinement of underlying protocols and the enhanced availability of specialized commercial systems enable us to investigate the microstructure of whole mouse organs and even allow for the characterization of cellular behavior in various live-cell imaging approaches. Here, we describe a protocol for the spatial whole-mount visualization and quantification of the $CD45^+$ leukocyte population in inflamed mouse hearts. The method employs a transgenic mouse strain (CD11c.DTR)that has recently been shown to serve as a robust, inducible model for the study of the development of fulminant fatal myocarditis, characterized by lethal cardiac arrhythmias. This protocol includes myocarditis induction, intravital antibody-mediated cell staining, organ preparation, and LSFM with subsequent computer-assisted image post-processing. Although presented as a highly-adapted method for our particular scientific question, the protocol represents the blueprint of an easily adjustable system that can also target completely different fluorescent structures in other organs and even in other species.

Video Link

The video component of this article can be found at https://www.jove.com/video/55450/

Introduction

During the evolution of light microscopy, many specialized forms appeared, all of them developed to minimize limitations in the visualization process for particular specimens. One such method is light-sheet fluorescence microscopy (LSFM). First developed in 1903 by Siedentopf and Zsigmondy[1] and finding its first fundamental biological applications in the early 1990s[2], LSFM has become the most powerful microscopic tool to date for the visualization of large specimens, such as intact mouse organs, with a fluorescence signal resolution down to the cellular level. Because of these benefits, in combination with its potential for live-cell imaging, Nature Methods named LSFM the "Method of the Year 2014[3]."

As the name suggests, the sample illumination in an LSFM is conducted by light sheets, which are orientated perpendicularly to the axis of the objective used for emission-light collection and subsequent image formation. The light sheet is usually generated either by focusing wide, collimated laser beams with a cylindrical lens or by the rapid sideways movement of narrow, focused laser beams in just one horizontal or vertical plane[4,5]. In this way, only the focal plane of the imaging optics is illuminated, typically with a thickness of 1-4 µm. Consequently, for a fluorescent sample placed in the illumination plane, both the generation of scattered light and the effects of photobleaching from regions above or below the focal plane are eliminated or greatly suppressed[6,7]. As all out-of-focus planes are not illuminated, photobleaching effects are omitted in these areas. In contrast to standard confocal or multi-photon microscopy, the paths of illuminated and emitted light are separate from each other, so the final image quality does not depend on the perfect focusing of the excitation light beam through the objectives. Depending on the underlying question, it is therefore possible to use objectives with an enormous field of view (FOV) so that the largest possible area of the illuminated plane can be imaged without any component parts moving in the xy-direction.

In modern LSFM systems, a fluorescent image of the generated optical section is captured on a highly sensitive charge-coupled device (CCD) or complementary metal-oxide semiconductor (CMOS) cameras, which are able to acquire the entire field of view (FOV) in microseconds. Therefore, by moving the sample through the light sheet and by acquiring images at defined z-steps, it is possible to obtain the full 3D information of a specimen in a reasonable amount of time[8,9], making this technique applicable for live-cell studies[10,11,12].

Nevertheless, although LSFM offers a rapid, sensitive, and fluorescence-friendly method, light transmission through the specimen is still a major issue, especially when large biological samples are the target for a 3D analysis. Light transmission is critically modified by physical aspects of absorption and by light scattering at interfaces of structures with different refractive indices[13]. Therefore, when imaging samples several millimeters in size, LSFM is mostly combined with clearing protocols to render the samples optically transparent. These techniques are based

on the idea of removing water from the respective biological tissue and exchanging it with water- or (organic) solvent-based immersion media, which are chosen to narrowly match the refractive indices of the particular target tissue components. As a result, lateral light scattering is minimized, and all wavelengths of light can much more efficiently pass through the tissue[13]. In many cases, biological specimens treated in this way appear macroscopically crystal-clear, which enables LSFM to be conducted, even on entire mouse organs, using long working-distance, low magnification objectives.

Here, we present a preparation protocol for large-sample imaging in a light-sheet microscope (see the table of materials), which we have established to investigate the cellular cardiac infiltrate in a murine model of myocarditis[15]. CD11c.DTR mice express the primate diphtheria toxin receptor (DTR) under the control of the CD11c promotor[16]. Consequently, cells in these mice, which express CD11c along with the DTR, are rendered sensitive to the exotoxin of *Corynebacterium diphtheria* (diphtheria toxin, DTX); the systemic treatment of these animals with DTX results in a depletion of all $CD11c^+$ cells. CD11c is an integrin and, as a cell-surface receptor for a variety of different soluble factors, is involved in activation and maturation processes mainly in cells of the monocytic lineage[17]. Consequently, the CD11c.DTR mouse model has been intensively used to study the role of dendritic cells and macrophage subsets in the context of many different immunological questions. Over time, it has been reported that CD11c.DTR mice treated systemically with DTX can develop adverse side effects and can display strongly elevated mortality rates[18,19]. Recently, we were able to identify the underlying cause of death[15], describing the development of fulminant myocarditis after intratracheal DTX application in these animals. The toxin challenge caused cellular destruction, including in central parts of the stimulus transmission system in the heart. This was accompanied by massive $CD45^+$ leukocyte infiltrate, finally leading to lethal cardiac arrhythmias. In this case, not only was the appearance of the leukocyte population important, but also its spatial distribution inside the heart. This experimental question is a challenge for modern microscopic imaging, which we have solved by a light-sheet microscopy approach that is supported by intravital antibody staining and an organic solvent-based optical clearing protocol.

Protocol

All animal experiments were conducted in accordance with EU guidelines and were approved by the relevant local authorities in Essen (AZ 84-02.04.2014.A036 - Landesamt für Natur, Umwelt und Verbraucherschutz Nordrhein-Westfalen, Essen, Germany). The animals were used and housed under specific pathogen-free (SPF) conditions.

1. Induction of Myocarditis by Diphtheria Toxin (DTX)

1. Prepare the DTX solution for the induction of myocarditis by diluting the DTX stock solution with phosphate-buffered saline (PBS) to a 1 µg/mL working solution.
2. **Apply 100 µL of this solution intratracheally (i.t.) into 8 to 10 week-old CD11c.DTR mice (*ca.* 5 ng/g bodyweight (bw)), as shown by Hasenberg *et al.* for the *i.t.* application of a fungal spore suspension[20].**
   NOTE: The intraperitoneal application of the toxin might result in a similar induction of fatal myocarditis. However, this approach would have to first be validated.
   1. For i.t. application, anesthetize the animals by an intraperitoneal (i.p.) injection of 100 mg/kg bw ketamine and 10 mg/kg bw xylazine.
   2. After reaching deep narcosis (toe pinch test), intubate the animals by using a 22 G indwelt venous catheter through the oral cavity. Check the correct positioning of the lens tube by ventilating the animals with a small-animal respirator at a rate of 250 breaths per min and an inhalation volume of 250 µL per breath, also shown by Hasenberg *et. al.*[20].
      NOTE: When positioned correctly, the breath rate of the animals will change according to the applied ventilation settings.
   3. Disconnect the ventilation system and instill the 100 µL of DTX solution or an equal amount of PBS as a control through the catheter into the lung and continue to ventilate the animals for 1 additional min.
3. Let the animals recover from anesthesia and monitor the general health status and body weight change for 4 days.
   NOTE: Depending on the genetic background, mouse strain, or initial weight, the severity and onset of myocarditis might vary and should be determined first.

2. Sample Preparation for Light-sheet Microscopy

1. 4 days after toxin application, anesthetize the mice by flushing an induction chamber with a vaporized 2% isoflurane/oxygen mixture. Inject 15 µg of a directly labeled anti-CD45 antibody (clone 30-F11, AlexaFluor647 (AF647)) in 50 µL of PBS intravenously (i.v.) using the retro-orbital application route, which ensures a very fast and highly accurate application of the correct amount of antibody.
   NOTE: The desired depth of narcosis has been reached when the mice are recumbent and do not react to toe pinch testing.
2. **After 2 h of incubation, sacrifice the mice by cervical dislocation and perfuse the hearts *in situ* with 5 mL of PBS/EDTA (5 mM).**
   1. Expose the heart and inject the perfusion solution into the right ventricle using a 21 G catheter. Perfuse with slow, constant pressure and make sure that the blood can be drained after cutting open the aorta.
      NOTE: This transcardial perfusion might result in minor preparation artifacts, which could disturb the final 3D visualization of the organ. Therefore, advanced animal experimenters could perform the perfusion through the inferior vena cava, excising the abdominal aorta.
3. **For chemical fixation, perfuse the heart through the same recess with 5 mL of 4% paraformaldehyde (PFA). Keep the catheter in place and simply attach a new syringe filled with PFA. Perfuse with slow and constant pressure.**
   NOTE: Paraformaldehydeis highly toxic; avoid contact with the skin, eyes, and other mucosa.
   1. Gently grasp the heart with serrated forceps; pull it slightly upwards; and cut all tissue connections, including the incoming and outgoing arteries and veins. Store the organ for an additional 4 h in 4% PFA for further fixation.
4. To dehydrate the organ, incubate the heart in an ascending ethanol series at 50%, 70%, and twice at 100%, each for 12 h, at 4 °C in the dark. Here, use black 5 mL polypropylene reaction tubes, allowing them to constantly rotate in a tube rotator using a slow rotation speed to prevent air-bubble formation.

5. Complete sample preparation by chemical clearing. To make the hearts transparent, incubate them in 98% dibenzyl ether (DBE) whilst constantly rotating overnight.
   NOTE: DBE is irritating to eyes, skin, and the respiratory system.

3. Light-sheet Microscopy

1. Conduct LSFM using the light-sheet microscope (see the table of materials). Place the sample on the standard sample holder of the microscope into the DBE-filled cuvette, which is suitable for specimens up to 30 mm x 30 mm x 15 mm.
2. **Hold the sample firmly in place during the image acquisition using dehydrated and cleared agarose blocks.**
   1. To prepare the agarose blocks, pour 2% molten agarose into a mold (15 mm x 15 mm x 5 mm). Let the agarose cool down until it solidifies.
   2. Dehydrate it in an ascending ethanol series (50%, 70%, and twice at 100%). Incubate the agarose blocks overnight in 98% DBE. Store the agarose in DBE until it is used.
      NOTE: As the agarose is comprised mainly of water, the incubation times for each dehydration step may be extended, depending on the size of the block.
      NOTE: DBE is irritating to the eyes, skin, and respiratory system.
   3. When needed, cut the prepared agarose block to the desired shape using a sharp scalpel. Typically, cut prism- or wedge-shaped forms to place at the edges of the sample adapter.
      NOTE: As the agarose blocks are elastic, the sample stays in place when pushed with little force.

3. **Detect the fluorescence signals of interest (here, autofluorescence and anti-CD45 antibody staining) with the appropriate excitation and emission filter settings.**
   1. For the detection of the connective tissue-derived autofluorescence signal, use a 525/50 nm bandpass filter at an excitation wavelength of 488 nm (OPSL: 50 mW); CD45 staining with an AF647-coupled antibody is detected at 668 nm (bandpass filter: 680/30 nm) and at an excitation wavelength of 647 nm (diode laser: 50 mW).
   2. Choose 4 µm as the distance between the two individual z-planes.

4. Image Post-processing

NOTE: The acquired digital image data were further processed with a scientific 3D/4D image processing and analysis software (see the table of materials).

1. **Opening and pre-adjustment of the data files.**
   1. After starting the analysis software, select the "Surpass" button in the upper-left corner. To open the image stacks, choose "File," "Open," and select a folder containing the data from the first acquired channel. Choose "Edit" and "Add Channels" to add further acquired channels.
      NOTE: Depending on the data size and the computer system, this process can take several minutes. The presented protocol demonstrates all steps for 2 acquisition channels (autofluorescence and AF647).
   2. Correct the x, y, and z voxel dimensions by clicking "Edit" and selecting "Image Properties." When the new window opens, adjust the parameters.
      NOTE: This step depends on the employed microscope system and the particular data format. Correct x-y-z values are critical for subsequent size and distant measurements. In most cases, these parameters are stored as meta data in the micrograph files. However, if the file format cannot be interpreted correctly by the analysis software, it is important to manually enter the pixel size. The pixel size in the x and y dimensions depend on the camera pixel size, the potentially applied binning, and the lens and objective magnification. The pixel size in z is equivalent to the self-defined z-step size (*e.g.,* 4 µm).

2. **Channel adjustments**
   1. First transform the autofluorescence signal to grayscale by opening the "Display adjustment" ("Edit" and "Show Display Adjustment"). A new window will list all opened channels and the display settings for all of them; to change its default color, select the autofluorescence channel and choose the "white" display style. Click "ok" to apply.
   2. For black level adjustment, go back to "Display adjustment" and adjust the black level value to exclude unwanted background signals that do not represent sample structures.
      1. To do so, use the upper-left triangle on the channel bar and drag it from left to right.
         NOTE: Changes will be visualized immediately. Make sure to only suppress signals not deriving from the sample. Minimum values in the background should never be "0" to avoid pitch-black pixels, as the noise signals might be needed for additional calculations. Make sure that all black level changes are performed after image acquisition. Otherwise, valuable sample information may be lost. The black-level adjustment just serves representative purposes. To use the same display settings over different samples, precise values can be entered into the "min" numerical field below the channel list. This is very helpful for quantitative analyses.

   3. Perform intensity adjustment, either by using the upper-right triangle to adjust the respective channel intensity or by entering precise values into the "max" numerical field below the channel list.
   4. Perform contrast adjustment by dragging the lower triangle in the middle of the channel bar to increase or decrease the gamma value or by entering the precise values.
   5. Adjust the AF647 channel according to the autofluorescence channel. As a difference, set the visualization of the AF647 signal to a heat-map color look-up table. Do this by choosing the channel mode "fire" in an approach similar to that in step 4.2.1.
      NOTE: As the overall signal intensities are significantly lower compared to the autofluorescence channel, the black levels are usually adjusted to much lower values. As for the autofluorescence channel, the brightness of this channel is usually increased.

6. Select the "blend mode" to visualize tissue structures in detail. Analyze all samples from one series with the same parameter values.

3. **Virtual clipping**
    1. To virtually cut open the organ before the 3D scene export, apply a clipping plane on the rendered 3D object.
        1. Click the "Clipping Plane" icon (scissors) in the object list. Inside the image view, a yellow frame and a manipulator (white spindle) will appear. Rotate the spindle at the thinner end with the mouse, thereby changing the orientation of the clipping plane, and move the thicker middle part of the spindle to select the desired depth of clipping.
        2. Hide the frame and manipulator by unchecking the respective checkboxes below the object list and create the desired snapshots.

Representative Results

The presented LSFM approach analyzes the leukocyte distribution and amount in murine hearts upon induction of severe myocarditis. **Figure 1A** explains the pre-treatment protocol for the transgenic CD11c.DTR mice for myocarditis induction. This step represents the necessary trigger for the recruitment of leukocytes to the myocardium. After successful DTX application, the animals develop severe disease symptoms, such as general weakness, anorexia, and weight loss within the range of 2-4 days. After 4 days, leukocytes are stained by the i.v. application of fluorochrome-coupled anti-CD45 antibody prior to transcardial perfusion to remove the blood from circulation. If performed successfully, the heart and other organs turn whitish. Subsequently, the organ is excised, and tissue water is exchanged with DBE by an ascending ethanol row and a final incubation in DBE. **Figure 1B** shows the timetable of the individual incubation steps in which the organ undergoes significant shrinkage. The chemically cleared organ is then transferred to a DBE-filled imaging chamber on the standard microscope tissue holder. To stabilize the organ during 3D image acquisition, it is fixed by transparent agarose blocks. The detailed positioning of the specimen is visualized in **Figure 2**. The acquisition of an entire image stack, composed of 2 channels (autofluorescence and anti-CD45), takes about 20-30 min and generates a data file of about 16 GB. Finally, the resulting data are analyzed as artificial 3D rendering in which the leukocyte distribution is displayed in a heatmap view. In **Figure 3** (upper row), the strongly inflamed areas of a heart of a DTX-treated animal can be perceived by their reddish/whitish appearance. A more detailed study of the 3D model reveals the leukocyte concentration, especially in regions of the cardiac conduction system, such as the atrioventricular bundle and the Purkinje fibers. In contrast, hearts of PBS-treated animals do not show this inflammation pattern at all (lower row).

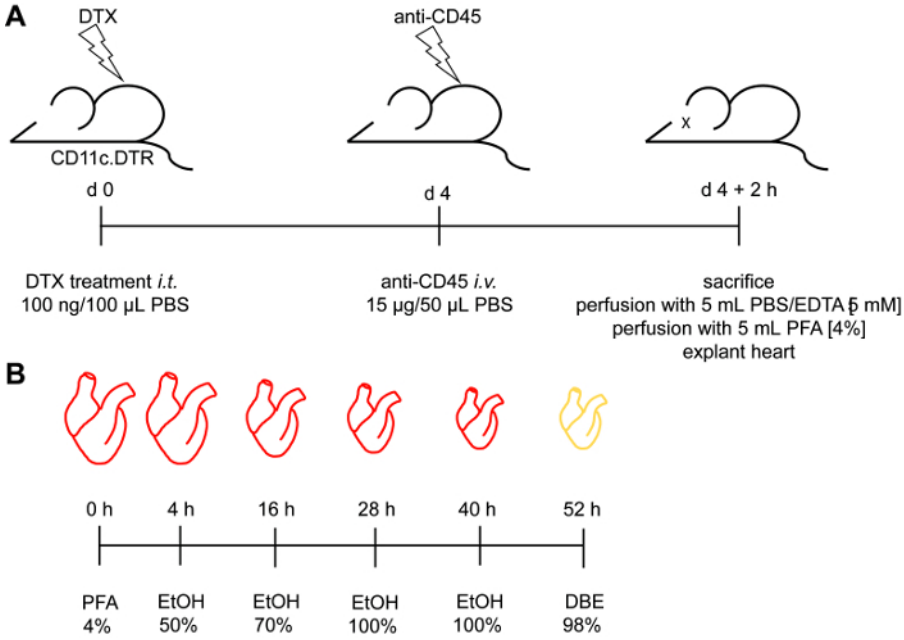

Figure 1: Scheme of Induction and Sample Preparation of Diphtheria Toxin-induced Myocarditis. (**A**) Myocarditis development was induced by the i.t. application of diphtheria toxin (100 ng/animal). After 4 days, myocarditis had fully developed and an AF647-coupled anti-CD45 antibody (15 µg/animal) was injected i.v. to detect $CD45^+$ leukocytes. Animals were sacrificed 2 h later by cervical dislocation, and the hearts were perfused with PBS/EDTA (5 mM) followed by 4% PFA. (**B**) After removal, the organ was dehydrated with an ascending ethanol series and finally cleared by overnight incubation in dibenzyl ether. Please click here to view a larger version of this figure.

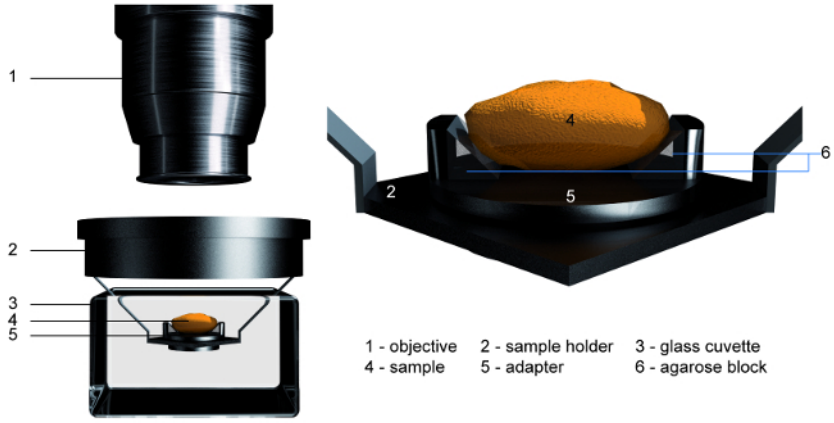

Figure 2: Scheme of Sample Positioning in the Microscope. The chemically cleared, transparent heart (4) was positioned on the sample holder (2 and 5) and stabilized with the help of cleared agarose blocks (6). This construct was then submerged in the DBE-filled glass cuvette (3). For acquisition, a 0.5 NA objective lens (1) with a working distance of 5.5 mm was employed. Please click here to view a larger version of this figure.

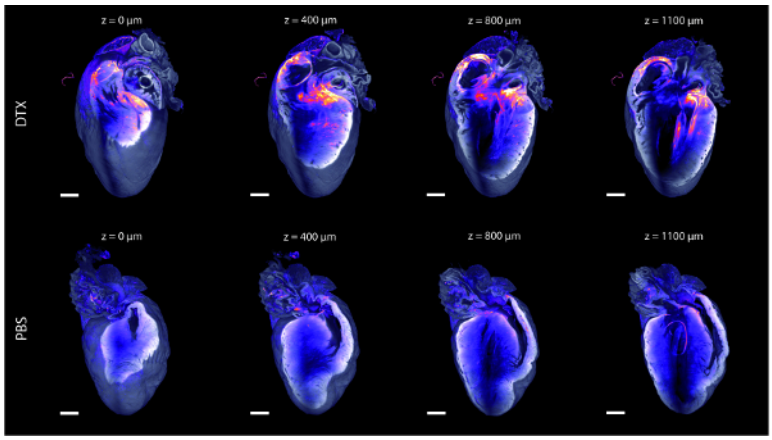

Figure 3: Representative 3D Renderings of Whole-organ Light-sheet Microscopy. CD11c.DTR mice were treated intratracheally with DTX (upper row) or PBS (lower row). 4 days later, the development of myocarditis, represented by $CD45^+$ leukocyte infiltration, was visualized by fluorescence light-sheet microscopy. To stain the $CD45^+$ cells, an anti-CD45 antibody coupled to AF647 was injected i.v. 2 h before sacrificing the mice. The autofluorescence signal of connective tissue is displayed in gray, whereas the $CD45^+$ infiltrate is shown in heatmap colors (blue: low signal; white: high signal). Each row is composed of 4 digitally clipped 3D renderings, demonstrating the situation inside the organ. The clipping depth relative to the front part of the heart is declared above the individual images. The figure has been modified from Mann *et al.*[15]. Scale bar = 1 mm. Please click here to view a larger version of this figure.

Discussion

In modern life science, the microscopic visualization of biological processes plays an increasingly important role. In this context, many developments have been achieved during the last two centuries that help to answer questions not addressable up to this point, . First, there has been a clear tendency to fundamentally increase the resolution ability of light microscopes. With structured illumination microscopy (SIM)[21,22], stimulated emission-depletion (STED) microscopy[23], and photo-activated localization microscopy (PALM)[24,25] or stochastic optical reconstruction microscopy (STORM)[26], the once-postulated resolution limitation due to light diffraction[27] was significantly broken. The second often-targeted challenge was to observe cellular behavior in an environment resembling the natural condition as closely as possible. In this context, the development of *in situ* or *in vivo* imaging approaches were forced. To overcome the limited light penetration depth in complex biological tissues, 2-photon microscopy[28,29] has set new standards in this research field.

However, a feature that all these microscopy techniques usually share is the use of high-NA objectives to guarantee the best possible resolution. Although it does resolve microstructures in greater detail, the use of high-NA objectives significantly restricts the field of view, as well as the working distance. As consequence, the biological context in terms of the surrounding environment often gets out of focus in the truest sense of the word. To close this gap, LSFM development has recently gained interest, providing a microscopy technique that is able to resolve fluorescent structures at cellular size but also to conveniently assess the entire 3D information of a specimen with a size of more than 1 cm.

The protocol described here presents a method of how to employ an ultramicroscope to visualize a cellular leukocyte infiltrate in entire murine hearts. After the successful induction of sterile myocarditis in a CD11c.DTR mouse model[30], the respective animal receives an i.v. injection of a fluorochrome-coupled anti-CD45 antibody, which circulates for 2 h in the living animal. In principle, by performing a post-mortem, the whole-mount antibody staining between organ fixation and sample dehydration should be possible. Unfortunately, whole-mount staining demands

much longer incubation steps and therefore massively increases the time needed for sample generation (*i.e.,* by 4-21 days)[6,31]. Furthermore, this intravital staining approach is not only faster, but also delivers more effective tissue penetration of the antibody compared to a whole-mount staining protocol[9]. Although the absolute staining efficiency has not been quantified, it is expected that a large proportion of the leukocyte population is labeled, given that the resulting fluorescence signal is remarkably strong. Both the fluorescent proteins and the antibody labeling itself largely survive the subsequent clearing process, and both appear to be stable for a long period of time. It should also be noted that a solvent-based agent is used for tissue clearing. This massively impedes a whole-mount staining approach following the clearing process. The solvent-based tissue clearing is a reversible phenomenon, so a transfer of the cleared tissue into a water-based medium (such as PBS), which is usually employed for standard antibody staining, would result in a non-transparent sample. Therefore, non-standard staining protocols in organic solvents would have to be established if a whole-mount staining procedure is needed after sample clearing.

The subsequent heart perfusion is absolutely necessary to eliminate as much residual blood as possible, since blood is poorly cleared in the following steps and dramatically worsens the imaging results. After excising the heart, the tissue water is removed in an ascending ethanol row. This step can be regarded as the first part of the chemical clearing. The idea is to substitute the tissue water with an immersion medium that better matches the mean refractive index (RI) of the specimen of choice. DBE was chosen as the immersion medium following the protocol of Ertuk *et al.*[32], with some modifications. DBE has a refractive index of 1.55 (nD20), and when it was compared to other clearing agents, such as benzyl alcohol:benzyl benzoate (BABB; RI (nD20) = 1.56)[6,7] or sucrose (RI (nD20) =1.44)[13], it best preserved the fluorescent labels used in this protocol. A similar fluorescence preservation was yielded using ethyl cinnamate (ECI). We have described its use in a study on the automated quantification of glomeruli in nephretic kidneys[9]. The muscle tissue, once estimated to have a refractive index of 1.382 ±0.004[33], was equally well cleared with all substances that we evaluated[9]. Therefore, the crucial factor for the choice of DBE was the fluorescence preservation and not the clearing potential. As a major change to this passive clearing protocol, the use of an active method such as CLARITY[34,35], where the removal of lipids with the aid of an electrophoretic current results in strongly cleared tissues, should be possible. However, in contrast to such a water-based clearing method, the DBE clearing results in a significant hardening of the tissue, accompanied with minor shrinkage. This allows for the easy handling of the samples and does not require further adaptions for imaging, such as embedding the sample in an agarose block. Therefore, the transfer of this protocol to a method like CLARITY would be challenging, but people have successfully demonstrated the use of the chosen ultramicroscope (see the table of materials) with this approach[3]. It is important to carefully evaluate the potential destruction of endogenous fluorescence signals by the clearing method of choice. As we have never worked with CLARITY or other active-clearing protocols, we cannot comment on the fluorochrome reaction in these systems. The worst case would be that a subsequent whole-mount antibody staining would have to be performed.

This method is easily adjustable to other organs, such as murine lungs; kidneys; brains; and even bones, such as the femur, tibia, or calvaria. While evaluating the application potential on new tissue regions and/or new fluorescent labeling strategies, the biggest challenge usually is to design the protocol in a way that the fluorescence is kept alive. The solvent-based immersion media[13] and the dehydration agents[36] have a direct impact on the integrity of the fluorochromes. The use of AlexaFluor derivatives are recommended, as they appear to be quite stable in various protocols. However, very often, other fluorochromes must be employed. In this case, it is definitely worth evaluating the use of other clearing agents (*e.g.,* Scale[37], Cubic[38], Succrose[13], Clarity[13,34], PACT[39], FocusClear[13], SeeDB[31], methyl salicylate[40], 3Disco[32], BABB[6], and ECI[9]) and other dehydration alternatives (*e.g.,* methanol and tetrahydrofurane[13]).

As in many other LSFM approaches, the process of positioning of the transparent heart under the microscope is demanding. Commercial systems provide enough space for installing samples the size of mouse organs, including lung lobes, kidneys, or hearts. However, at the moment, no standardized sample holders for these specimens are available. Therefore, we had to establish a mounting apparatus by using cleared and re-shaped agarose blocks. Still, a certain number of image data sets had to be discarded due to movement artifacts. This problem was also increased due to the long acquisition time of the microscope used here. Potentially, the generation of huge data sets will profit significantly from faster systems, but we did not have the chance to use a faster microscope yet. Our microscope (see table of materials) was built around a zoom microscope body and was equipped with a laser module, an sCMOS camera with a pixel size of 6.5 x 6.5 mm^2, and detection optics with an optical magnification range from 1.26X to 12.6X. The central part of the detection optics was a 0.5 NA objective lens with a working distance of 5.5 mm, which allowed for the observation of a large field of view ranging between 1.7 and 17.6 mm diagonally. This was large enough to perform the optical sectioning of entire murine hearts. The correction of chromatic aberration, between 400 and 800 nm, was achieved by the mechanical adjustment of the objective. Where needed, chromatic corrections were further performed during the computer-assisted post-processing. Spherical aberration, also in thicker specimens, were not observed in this system and therefore did not have to be corrected.

All in all, we present here a robust protocol for the chemical clearing and analysis of spatial leukocyte distribution inside murine hearts using light-sheet microscopy. At this point, it is important to emphasize that this LSFM procedure is hardly able to resolve fine tissue structures such as capillaries. In this respect, this LSFM is well-suited to characterize the general immune cell distribution and to describe potential immune cell accumulations inside the organ. However, one must keep in mind that LSFM in general is not the perfect choice for analyzing and quantifying cellular localization in small-organ sub-structures, such as the vasculature. To answer such questions, LSFM should be complemented with other methods, such as histology or 2-photon microscopy. Further limitations of this protocol include the restriction to a maximum of 3-4 colors-the blue channel is hard to use for other signals apart from autofluorescence-the restriction to fixed samples, and the maximum sample size of 30 mm x 30 mm x 15 mm. Also, the strong smell and the acute toxicity of DBE should be taken into account. If the latter point is problematic, ethyl cinnamate can be used as an alternative clearing agent[9]. The major advantage of choosing of this microscopy technique is the ability to analyze the entire organ at once. In conventional analyses of hematoxylin and eosin-stained, formalin-fixed, and paraffin-embedded (FFPE) histological tissue sections, there is a high likelihood of missing important spatial areas unless every single section is analyzed. Moreover, light-sheet microscopy not only enables virtual cutting of the sample in every three-dimensional plane, but it also offers this potential without destroying the specimen or causing cutting artifacts. If needed, the fixed organ could subsequently be processed for further analyses, such as a correlative light and electron microscopy approaches to highly resolve particular regions of interest. A template for such a study can be found in the work of Karreman *et al.*, where the correlation between a 2-photon microscopy image stack and three-dimensional electron microscopy data was successfully shown[41]. Another promising approach could be the combination of this protocol with the recently published uDISCO method that is also based on an organic solvent and that would allow for the investigation of much bigger organs by a standard LSFM[42].

Disclosures

The authors have nothing to disclose.

Acknowledgements

Research in the Gunzer laboratory was supported by the German Federal Ministry of Education and Research (grant no. 0315590 A-D) and by the German Research Foundation (grant no. GU769/4-1, GU769/4-2). We further thank the IMCES for technical support and Sebastian Kubat for help with 3D cartoon modeling.

References

1. Siedentopf, H., & Zsigmondy, R. Uber Sichtbarmachung und Größenbestimmung ultramikoskopischer Teilchen, mit besonderer Anwendung auf Goldrubingläser. *Annalen der Physik.* **315** (1), 1-39 (1902).
2. Voie, A.H., Burns, D.H., & Spelman, F.A. Orthogonal-plane fluorescence optical sectioning: three-dimensional imaging of macroscopic biological specimens. *J. Microsc.* **170** (Pt 3), 229-236 (1993).
3. Epp, J.R. *et al.* Optimization of CLARITY for Clearing Whole-Brain and Other Intact Organs(1,2,3). *eNeuro.* **2** (3) (2015).
4. Greger, K., Swoger, J., & Stelzer, E.H. Basic building units and properties of a fluorescence single plane illumination microscope. *Rev. Sci. Instrum.* **78** (2), 023705 (2007).
5. Keller, P.J., & Stelzer, E.H. Digital scanned laser light sheet fluorescence microscopy. *Cold Spring Harb Protoc.* **2010** (5), pdb top78 (2010).
6. Becker, K., Jahrling, N., Kramer, E.R., Schnorrer, F., & Dodt, H.U. Ultramicroscopy: 3D reconstruction of large microscopical specimens. *J Biophotonics.* **1** (1), 36-42 (2008).
7. Dodt, H.U. *et al.* Ultramicroscopy: three-dimensional visualization of neuronal networks in the whole mouse brain. *Nat. Methods.* **4** (4), 331-336 (2007).
8. Taormina, M.J. *et al.* Investigating bacterial-animal symbioses with light sheet microscopy. *Biol. Bull.* **223** (1), 7-20 (2012).
9. Klingberg, A. *et al.* Fully Automated Evaluation of Total Glomerular Number and Capillary Tuft Size in Nephritic Kidneys Using Lightsheet Microscopy. *J. Am. Soc. Nephrol.* (2016).
10. Truong, T.V., Supatto, W., Koos, D.S., Choi, J.M., & Fraser, S.E. Deep and fast live imaging with two-photon scanned light-sheet microscopy. *Nat. Methods.* **8** (9), 757-760 (2011).
11. Schmid, B. *et al.* High-speed panoramic light-sheet microscopy reveals global endodermal cell dynamics. *Nat Commun.* **4**, 2207 (2013).
12. Cella Zanacchi, F. *et al.* Live-cell 3D super-resolution imaging in thick biological samples. *Nat. Methods.* **8** (12), 1047-1049 (2011).
13. Richardson, D.S., & Lichtman, J.W. Clarifying Tissue Clearing. *Cell.* **162** (2), 246-257 (2015).
14. Maruyama, A. *et al.* Wide field intravital imaging by two-photon-excitation digital-scanned light-sheet microscopy (2p-DSLM) with a high-pulse energy laser. *Biomed Opt Express.* **5** (10), 3311-3325 (2014).
15. Männ, L. *et al.* CD11c.DTR mice develop a fatal fulminant myocarditis after local or systemic treatment with diphtheria toxin. *Eur. J. Immunol.* **46** (8), 2028-2042 (2016).
16. Jung, S. *et al.* In vivo depletion of CD11c+ dendritic cells abrogates priming of CD8+ T cells by exogenous cell-associated antigens. *Immunity.* **17** (2), 211-220 (2002).
17. Corbi, A.L., & Lopez-Rodriguez, C. CD11c integrin gene promoter activity during myeloid differentiation. *Leuk. Lymphoma.* **25** (5-6), 415-425 (1997).
18. Zaft, T., Sapoznikov, A., Krauthgamer, R., Littman, D.R., & Jung, S. CD11chigh dendritic cell ablation impairs lymphopenia-driven proliferation of naive and memory CD8+ T cells. *J. Immunol.* **175** (10), 6428-6435 (2005).
19. Zammit, D.J., Cauley, L.S., Pham, Q.M., & Lefrancois, L. Dendritic cells maximize the memory CD8 T cell response to infection. *Immunity.* **22** (5), 561-570 (2005).
20. Hasenberg, M., Kohler, A., Bonifatius, S., Jeron, A., & Gunzer, M. Direct observation of phagocytosis and NET-formation by neutrophils in infected lungs using 2-photon microscopy. *J. Vis. Exp.* (52) [doi] (2011).
21. Bailey, B., Farkas, D.L., Taylor, D.L., & Lanni, F. Enhancement of axial resolution in fluorescence microscopy by standing-wave excitation. *Nature.* **366** (6450), 44-48 (1993).
22. Gustafsson, M.G. Surpassing the lateral resolution limit by a factor of two using structured illumination microscopy. *J. Microsc.* **198** (Pt 2), 82-87 (2000).
23. Hell, S.W., & Wichmann, J. Breaking the diffraction resolution limit by stimulated emission: stimulated-emission-depletion fluorescence microscopy. *Opt Lett.* **19** (11), 780-782 (1994).
24. Betzig, E. *et al.* Imaging intracellular fluorescent proteins at nanometer resolution. *Science.* **313** (5793), 1642-1645 (2006).
25. Hess, S.T., Girirajan, T.P., & Mason, M.D. Ultra-high resolution imaging by fluorescence photoactivation localization microscopy. *Biophys. J.* **91** (11), 4258-4272 (2006).
26. Rust, M.J., Bates, M., & Zhuang, X. Sub-diffraction-limit imaging by stochastic optical reconstruction microscopy (STORM). *Nat. Methods.* **3** (10), 793-795 (2006).
27. Abbe, E. Beiträge zur Theorie des Mikroskops und der mikroskopischen Wahrnehmung. *Archiv für mikroskopische Anatomie.* **9** (1), 413-418 (1873).
28. Göppert-Mayer, M. Über Elementarakte mit zwei Quantensprüngen. *Annalen der Physik.* **401** (3), 273-294 (1931).
29. Denk, W., Strickler, J.H., & Webb, W.W. Two-photon laser scanning fluorescence microscopy. *Science.* **248** (4951), 73-76 (1990).
30. Männ, L. *et al.* CD11c.DTR mice develop a fatal fulminant myocarditis after local or systemic treatment with diphtheria toxin. *Eur. J. Immunol.* In press. (2016).
31. Ke, M.T., Fujimoto, S., & Imai, T. SeeDB: a simple and morphology-preserving optical clearing agent for neuronal circuit reconstruction. *Nat. Neurosci.* **16** (8), 1154-1161 (2013).
32. Erturk, A. *et al.* Three-dimensional imaging of solvent-cleared organs using 3DISCO. *Nat. Protoc.* **7** (11), 1983-1995 (2012).

33. Dirckx, J.J., Kuypers, L.C., & Decraemer, W.F. Refractive index of tissue measured with confocal microscopy. *J Biomed Opt.* **10** (4), 44014 (2005).
34. Chung, K. *et al.* Structural and molecular interrogation of intact biological systems. *Nature*. **497** (7449), 332-337 (2013).
35. Tomer, R., Ye, L., Hsueh, B., & Deisseroth, K. Advanced CLARITY for rapid and high-resolution imaging of intact tissues. *Nat. Protoc.* **9** (7), 1682-1697 (2014).
36. Schwarz, M.K. *et al.* Fluorescent-protein stabilization and high-resolution imaging of cleared, intact mouse brains. *PLoS One.* **10** (5), e0124650 (2015).
37. Hama, H. *et al.* Scale: a chemical approach for fluorescence imaging and reconstruction of transparent mouse brain. *Nat. Neurosci.* **14** (11), 1481-1488 (2011).
38. Susaki, E.A. *et al.* Whole-brain imaging with single-cell resolution using chemical cocktails and computational analysis. *Cell.* **157** (3), 726-739 (2014).
39. Yang, B. *et al.* Single-cell phenotyping within transparent intact tissue through whole-body clearing. *Cell.* **158** (4), 945-958 (2014).
40. Shivapathasundharam, B., & Berti, A.E. Transparent tooth model system. An aid in the study of root canal anatomy. *Indian J. Dent. Res.* **11** (3), 89-94 (2000).
41. Karreman, M.A. *et al.* Fast and precise targeting of single tumor cells in vivo by multimodal correlative microscopy. *J. Cell Sci.* **129** (2), 444-456 (2016).
42. Pan, C. *et al.* Shrinkage-mediated imaging of entire organs and organisms using uDISCO. *Nat. Methods.* **13** (10), 859-867 (2016).

